Prediction of process-induced deformation in CF/LM-PAEK thermoplastic composite laminates at different cooling rates

K. Ryuzono[1*], T. Shimizu[1], S. Koo[1], S. Mishima[1], and T. Okabe[1,2,3]

[1] Department of Aerospace Engineering, Tohoku University, Sendai, Miyagi, Japan,
[2] Department of Materials Science and Engineering, University of Washington, Seattle, WA, USA,
[3] Research Center for Structural Materials, Polymer Matrix Hybrid Composite Materials Group, National Institute for Materials Science, Tsukuba, Ibaraki, Japan

* *Corresponding author (ryuzono@tohoku.ac.jp)*

Keywords: *Carbon-fiber-reinforced thermoplastics; Process-induced deformation; Cooling rates; Crystallization; Finite element analysis*

Abstract

Carbon-fiber-reinforced thermoplastics are promising for high-rate production of next-generation single-aisle aircraft structures, but their process-induced deformation (PID) remains difficult to predict because crystallinity and mechanical properties depend strongly on cooling rate. This study investigates cooling-rate-dependent PID in T700G/LM-PAEK laminates and identifies key modeling requirements for predictive finite element (FE) analysis. Laminates were fabricated under six cooling-rate conditions from 5 to 71 °C/min. PID was measured by three-dimensional scanning, crystallinity was evaluated by differential scanning calorimetry (DSC), and initial stiffness and viscoelastic properties were characterized by dynamic mechanical analysis. The measured PID, crystallinity, and initial stiffness all decreased with increasing cooling rate, indicating that reduced crystallinity lowers both laminate stiffness and crystallization-induced shrinkage strain, thereby reducing residual stress. An anisotropic viscoelastic FE analysis incorporating cooling-rate-dependent stiffness and crystallization-induced shrinkage reproduced the experimentally observed decrease in PID with increasing cooling rate. Additional DSC measurements showed that the crystallization onset temperature decreased with increasing cooling rate, suggesting that the stiffness-development temperature should also be modeled as cooling-rate dependent to improve PID prediction.

1. Introduction

For high-rate production of next-generation single-aisle aircraft structures, carbon-fiber-reinforced thermoplastics (CFRTPs) have attracted considerable attention because of their short molding cycles, excellent mechanical properties, and potential for reheating and welding. Shorter molding cycles, including high-rate cooling, are essential for improving the productivity of CFRTP manufacturing. However, the cooling rate strongly affects the crystallization process of

semicrystalline thermoplastic resins, thereby changing the degree of crystallinity, stiffness, and crystallization-induced shrinkage [1]. Consequently, the residual stress and process-induced deformation (PID) generated during molding also depend on the cooling conditions.

To ensure the dimensional accuracy of composite structures, it is important to predict PID in advance. Experimental and numerical studies have investigated spring-in, spring-out, warpage, and residual stress in CFRTPs [2–5]. The effects of cooling rate on the crystallinity and mechanical properties of CFRTP laminates have also been reported [6,7]. However, few studies have systematically evaluated PID in CFRTP laminates fabricated under well-controlled high-cooling-rate conditions and examined the governing factors through finite element (FE) analysis.

This study investigates T700G/LM-PAEK (TC1225, Toray Advanced Composites), a CFRTP system of growing interest for aircraft structural applications, to clarify the effect of cooling rate on PID and identify the factors required for its prediction. Laminates were fabricated by press molding using temperature-controlled molds under conditions ranging from the manufacturer-recommended profile to high cooling rates, and their PID was evaluated. The degree of crystallinity, initial stiffness, and viscoelastic properties were then measured using differential scanning calorimetry (DSC) and dynamic mechanical analysis (DMA) to identify the factors governing PID. Finally, anisotropic viscoelastic FE analyses incorporating cooling-rate-dependent stiffness and crystallization-induced shrinkage were performed to examine whether the experimentally observed cooling-rate dependence of PID could be reproduced.

2. Experimental methods

This section describes the fabrication conditions and experimental procedures used to evaluate PID, crystallinity, and temperature-dependent stiffness. The obtained properties are used as inputs for the FE analyses described in Section 3.

2.1. Fabrication of T700G/LM-PAEK laminates at different cooling rates

Figure 1a shows the press system and molds used to fabricate T700G/LM-PAEK laminates at different cooling rates. An electric servo press (ZENFormer MPS675DS, Hoden Seimitsu Kako Kenkyusho Co., Ltd.) was used to apply pressure to the laminates. Molds designed to produce 150 mm × 150 mm laminates were used, and heating and cooling of the molds were regulated using a temperature-control system (Go Molding System II, Go Factory Co., Ltd.). The laminates were first heated from room temperature to 365 °C at 170 °C/min under a pressure of less than approximately 1 MPa. Three minutes after reaching the maximum temperature, a pressure of 5 MPa was applied and maintained for 5 min. The laminates were then cooled to 30 °C at a prescribed cooling rate while maintaining the pressure.

Figure 1b shows the temperature profiles obtained during preliminary molding trials under six prescribed cooling-rate conditions. These profiles represent the average of eight temperature histories measured by temperature sensors, four installed on the upper mold and four on the lower mold. Based on these temperature histories, the actual cooling rates calculated between 350 °C

and 150 °C were 5, 20, 40, 58, 66, and 71 °C/min. Using these molding conditions, T700G/LM-PAEK laminates with a [0/90] stacking sequence were fabricated for PID and DSC measurements, whereas $[0]_{16}$ laminates were fabricated for DMA measurements.

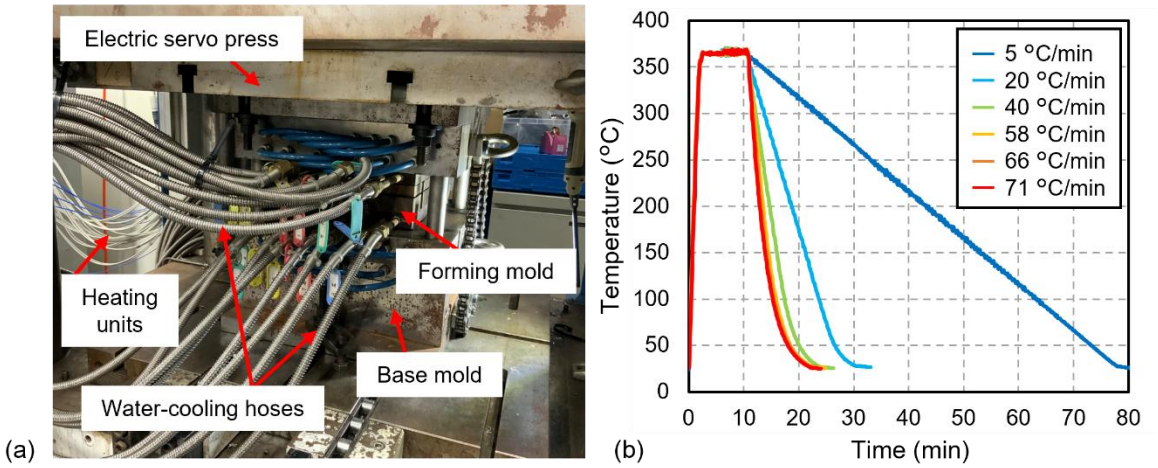

Figure 1. Fabrication of T700G/LM-PAEK cross-ply laminates: (a) electric servo press with temperature-controlled molds; (b) temperature profiles under six cooling-rate conditions.

2.2. PID measurements, DSC, and DMA

The distribution of out-of-plane deformation in the fabricated [0/90] laminates was measured using a three-dimensional blue-light scanner (VL-550, Keyence). An offset plane was defined from four points near the center of each laminate, and the difference between the minimum and maximum out-of-plane displacements from this plane was defined as the PID.

The degree of crystallinity of the specimens fabricated at each cooling rate was then measured using DSC (DSC600, Hitachi High-Tech Corporation). After the PID measurements, small specimens were cut from five locations in each laminate and used for the DSC measurements. The heat absorbed during crystal melting was measured, and the degree of crystallinity, X_c, was calculated using the following equation:

$$X_{\mathrm{c}} = \frac{\Delta H_{\mathrm{m}}}{(1 - W_{\mathrm{f}})\Delta H_{\mathrm{m}}^{0}}, \tag{1}$$

where ΔH_{m} denotes the melting enthalpy per unit mass. $\Delta H_{\mathrm{m}}^{0}$ denotes the melting enthalpy per unit mass of fully crystalline LM-PAEK resin, which was taken as 130 J/g [8]. W_{f} is the carbon-fiber weight fraction, which was set to 0.66 based on the manufacturer's datasheet [9]. ΔH_{m} was determined from the area of the endothermic peak at the melting temperature in the DSC curves and was used to calculate the degree of crystallinity. The DSC measurements were conducted over a temperature range of 20–365 °C at a heating rate of 10 °C/min.

The viscoelastic properties of the specimens fabricated at each cooling rate were measured using DMA (DMA7100, Hitachi High-Tech Corporation). Specimens with dimensions of 50 mm × 10

mm were cut such that the fiber direction was oriented at 90° or 45° with respect to the loading direction. To determine the initial stiffness, the storage modulus was measured at room temperature for 5 min at a frequency of 1 Hz, and the average storage modulus was calculated. The viscoelastic properties were evaluated using the 90° specimens over a temperature range of 20–250 °C at a heating rate of 0.5 °C/min and frequencies of 0.1–10 Hz. The obtained temperature–storage modulus curves were normalized by the storage modulus at 20 °C. Master curves were then constructed based on the time–temperature superposition principle (TTSP).

3. Numerical methods

Anisotropic viscoelasticity must be considered to predict the PID of composite laminates [3,4,10]. Because the cooling rate changes the degree of crystallinity, stiffness, and crystallization-induced shrinkage strain in CFRTP laminates, the FE analysis developed in a previous study [3] was extended to incorporate these cooling-rate-dependent properties. This section focuses on these additional considerations; details of the underlying numerical method are provided in Ref. [3].

3.1. Formulation of FE analysis

The relaxation moduli in the anisotropic viscoelastic constitutive model were introduced into the FE analysis by fitting the DMA-derived master curves to a generalized Maxwell model (GMM). When the GMM is represented by N Maxwell elements connected in parallel, the relaxation modulus $C_{ij}(t)$ at time t is given by

$$\begin{aligned} C_{ij}(t) &= C_{ij}^0 - \sum_{r=1}^{N} C_{ij}^r \left[1 - \exp\left(-\frac{t}{\alpha_{ij}(T)\tau_{ij}^r}\right)\right] \\ &= C_{ij}^0 \left(1 - \sum_{r=1}^{N} \bar{C}_{ij}^r \left[1 - \exp\left(-\frac{t}{\alpha_{ij}(T)\tau_{ij}^r}\right)\right]\right). \end{aligned} \tag{2}$$

Here, C_{ij}^r represents the spring constant of the Maxwell element, and C_{ij}^0 denotes the initial stiffness $C_{ij}(0)$. τ_{ij}^r is the relaxation time defined as η_{ij}^r / C_{ij}^r, where η_{ij}^r is the coefficient of viscosity of the Maxwell element. $\alpha_{ij}(T)$ denotes the shift factor at temperature T in the TTSP. As shown in Eq. (2), the relaxation modulus $C_{ij}(t)$ can be expressed as the product of the initial stiffness C_{ij}^0 and a normalized relaxation function. In this representation, the stiffness change caused by the cooling rate is reflected in C_{ij}^0, whereas the time-dependent relaxation response is described by the normalized relaxation function. Therefore, if the normalized relaxation function is assumed to be nearly independent of the cooling rate, the GMM parameters can be identified from the master curve obtained under a single cooling-rate condition. The relaxation modulus $C_{ij}(t)$ corresponding to each cooling rate can then be calculated using these GMM parameters together with the initial stiffness C_{ij}^0 of the laminate fabricated at the target cooling rate.

During the molding process of CFRTP laminates, the thermoplastic resin undergoes both thermal and crystallization-induced shrinkage. Although only thermal shrinkage was considered in the previous study [3], crystallization-induced shrinkage is additionally incorporated in the present study. The non-mechanical strain increment $\Delta \boldsymbol{E}^{\mathrm{nm}}$ consists of the thermal shrinkage strain increment $\Delta \boldsymbol{E}^{\mathrm{th}}$ and the crystallization-induced shrinkage strain increment $\Delta \boldsymbol{E}^{\mathrm{cr}}$ as follows:

$$\Delta \boldsymbol{E}^{\mathrm{nm}} = \begin{cases} \Delta \boldsymbol{E}^{\mathrm{th}} = [\beta_1^{\mathrm{th}} \Delta T \quad \beta_2^{\mathrm{th}} \Delta T \quad \beta_3^{\mathrm{th}} \Delta T \quad 0 \quad 0 \quad 0]^{\mathrm{T}} \\ \Delta \boldsymbol{E}^{\mathrm{cr}} = [\Delta E_1^{\mathrm{cr}} \quad \Delta E_2^{\mathrm{cr}} \quad \Delta E_3^{\mathrm{cr}} \quad 0 \quad 0 \quad 0]^{\mathrm{T}}, \end{cases} \tag{3}$$

where the Cartesian and material coordinate systems are denoted by $x - y - z$ and $1 - 2 - 3$, respectively, with 1, 2, and 3 corresponding to the fiber, transverse, and through-thickness directions. Here, β_j^{th} is the CTE in the j-direction, ΔT is the temperature increment in each simulation step, and ΔE_j^{cr} is the crystallization-induced shrinkage strain increment, calculated by dividing the total crystallization-induced shrinkage strain γ_j^{cr} by the number of simulation steps over the crystallization temperature range. In this study, the CTE was taken from the value reported in the previous study [3] for a cooling rate of 5 °C/min, regardless of the cooling rate considered. The total crystallization-induced shrinkage strain γ_j^{cr} was calculated using the resin stiffness corresponding to each cooling rate, based on the following equations [5]:

$$\gamma_1^{\mathrm{cr}} = \frac{\gamma_{\mathrm{m}} E_{\mathrm{m}} (1 - V_{\mathrm{f}})}{E_{1,\mathrm{f}} V_{\mathrm{f}} + E_{\mathrm{m}} (1 - V_{\mathrm{f}})}, \tag{4}$$

$$\gamma_2^{\mathrm{cr}} = \gamma_3^{\mathrm{cr}} = (1 + \nu_{\mathrm{m}}) \gamma_{\mathrm{m}} (1 - V_{\mathrm{f}}) - \nu_{12} \gamma_1^{\mathrm{cr}}, \tag{5}$$

where γ_{m} is the total crystallization-induced shrinkage strain of the resin. E and ν are the elastic modulus and Poisson's ratio, respectively, and the subscripts f and m denote the fiber and matrix, respectively. V_{f} is the fiber volume fraction. The elastic modulus and Poisson's ratio of the resin were determined using a self-consistent micromechanics model [3] from the DMA-measured moduli of the specimens with 90° and 45° fiber orientations. The total crystallization-induced shrinkage strain of the resin, γ_{m}, was taken as 0.05 based on the literature [11], regardless of the cooling rate.

3.2. FE model

Figure 2 shows the FE model used in this study. Considering symmetry, one-quarter of the experimentally fabricated specimen was modeled. The model dimensions were 75 mm × 75 mm × 0.3 mm. Twenty-node quadratic hexahedral elements were used, with an element size of 1 mm × 1 mm × 0.15 mm. The boundary conditions were set in the same manner as in the previous study [3]. During the molding process, the bottom surface of the model was fixed, and pressure was applied to the top surface. In the final step, both the pressure and the fixed boundary condition were released, and only the origin was constrained. For numerical stability, an initial cylindrical imperfection was introduced in the z-direction. The analysis was performed during cooling from 188 to 30 °C, as in the previous study [3].

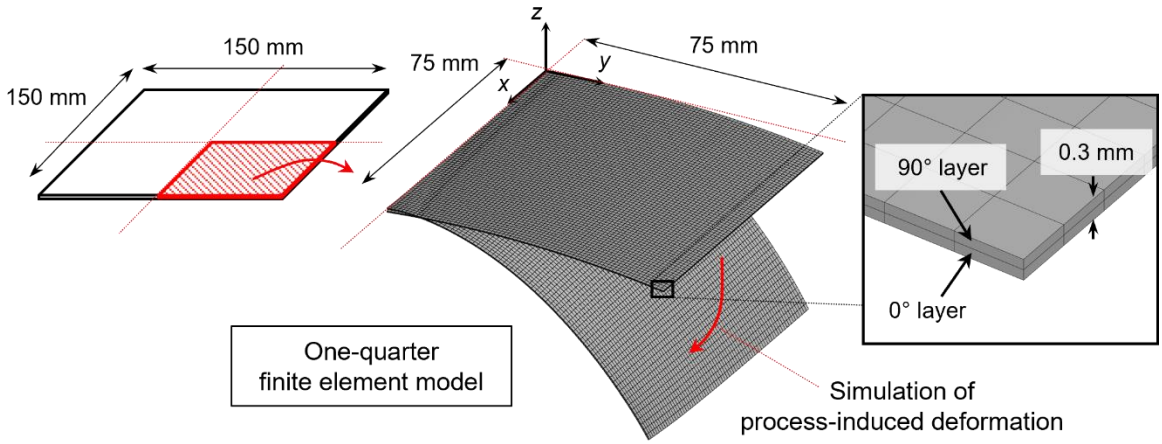

Figure 2. FE model for predicting PID in CFRTP cross-ply laminates.

4. Results and discussion

This section first discusses the cooling-rate dependence of crystallinity and stiffness based on DSC and DMA measurements. The relationship between experimentally measured PID and cooling rate is then compared with the numerical results. Possible reasons for the discrepancy between the experimental and numerical results are examined based on additional DSC measurements.

4.1. Crystallinity and storage modulus measured by DSC and DMA

Figure 3a shows the degree of crystallinity calculated from DSC measurements of T700G/LM-PAEK laminates fabricated under the six cooling-rate conditions. Because the DSC specimens were small, local variations in V_f likely caused the relatively large scatter in the calculated crystallinity. Nevertheless, the average crystallinity decreased with increasing cooling rate, as reported for CFRTP systems based on matrices such as PEEK and PPS [6,7]. Figure 3b shows the initial storage modulus obtained from DMA measurements. For both the 90° and 45° specimens, the initial storage modulus decreased as the cooling rate increased. This reduction is attributed to the lower crystallinity, which decreased the fraction of the high-modulus crystalline phase and increased that of the low-modulus amorphous phase, consistent with previous reports on other CFRTP materials [6,7].

Figure 4a shows the storage modulus curves obtained from temperature-sweep DMA measurements at 1 Hz, normalized by the storage modulus at 20 °C. The normalized curves were broadly similar among the cooling-rate conditions; however, the relative magnitude of the normalized storage modulus reversed around the glass transition temperature T_g of T700G/LM-PAEK, 147 °C [9]. Below T_g, the earlier decrease in the normalized storage modulus for the low-cooling-rate specimens may be related to local stress concentration in the amorphous regions confined between crystalline phases. This interpretation is consistent with the authors' previous fiber–matrix-scale analysis [4], which showed that stress concentration in resin-rich regions can

promote local stress relaxation. Above T_g, the molecular mobility of the amorphous phase becomes more pronounced, and the crystalline phase is expected to constrain large-scale molecular motion. This constraint may suppress the modulus reduction in specimens with higher crystallinity, resulting in a more gradual decrease in the normalized storage modulus at elevated temperatures. Figure 4b shows the master curves constructed from temperature- and frequency-sweep DMA measurements, normalized by the storage modulus at 20 °C and 1 Hz. This tendency was also observed in the normalized master curves, where the storage modulus decreased more gradually for specimens fabricated at lower cooling rates.

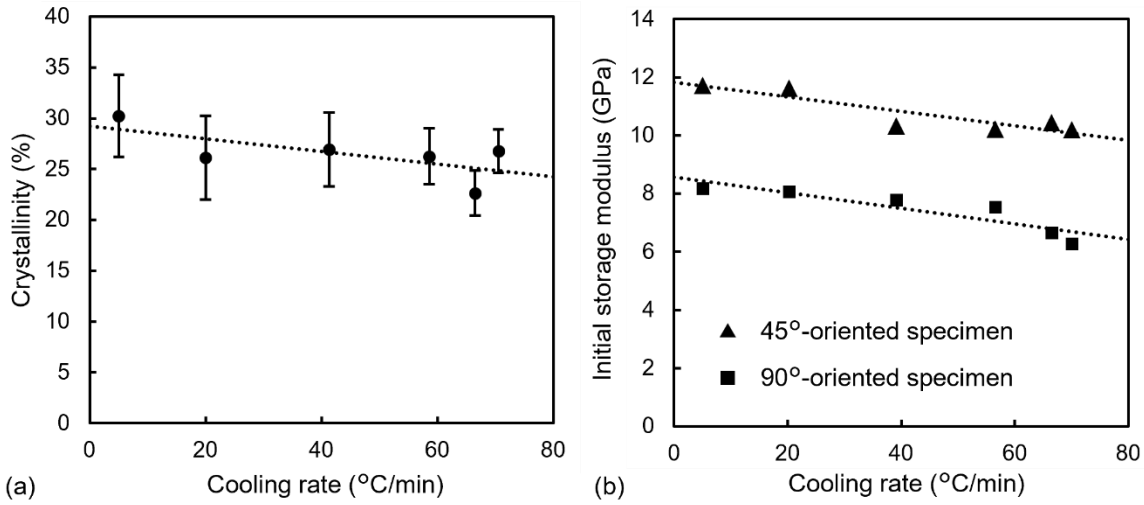

Figure 3. Experimental results obtained from DSC and DMA measurements: (a) crystallinity and (b) initial storage modulus of T700G/LM-PAEK laminates fabricated at different cooling rates.

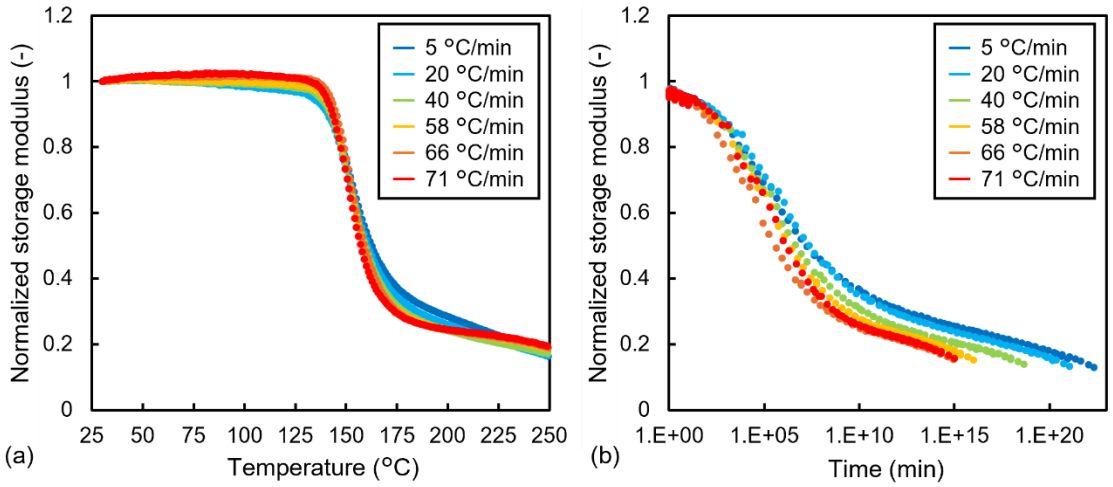

Figure 4. Experimental results obtained from DMA measurements of 90° specimens of T700G/LM-PAEK fabricated at different cooling rates: (a) storage modulus curves at a frequency of 1 Hz and (b) master curves normalized by the initial storage modulus at 20 °C and 1 Hz.

4.2. Numerical and experimental results of PID in T700G/LM-PAEK laminates

The results in Section 4.1 showed that both the degree of crystallinity and stiffness decreased with increasing cooling rate. Based on these findings, this section presents the FE analysis results for PID prediction accounting for cooling-rate-dependent stiffness and crystallization-induced shrinkage. Although the temperature- and time-dependent storage modulus showed slight differences among the cooling-rate conditions, the present analysis assumed, for simplicity, that only the initial stiffness depended on the cooling rate. The normalized storage modulus curve obtained at 5 °C/min was fitted to a GMM, and the fitted parameters were used to calculate the relaxation moduli for all cooling-rate conditions.

Figure 5 shows the experimentally measured and numerically predicted PID values for the six cooling-rate conditions. The experimental PID decreased with increasing cooling rate. This decrease is attributed to the lower degree of crystallinity at higher cooling rates, which reduced both the laminate stiffness and crystallization-induced shrinkage strain, thereby decreasing the residual stress and the resulting PID. The FE analysis reproduced this experimental trend by incorporating these cooling-rate-dependent properties.

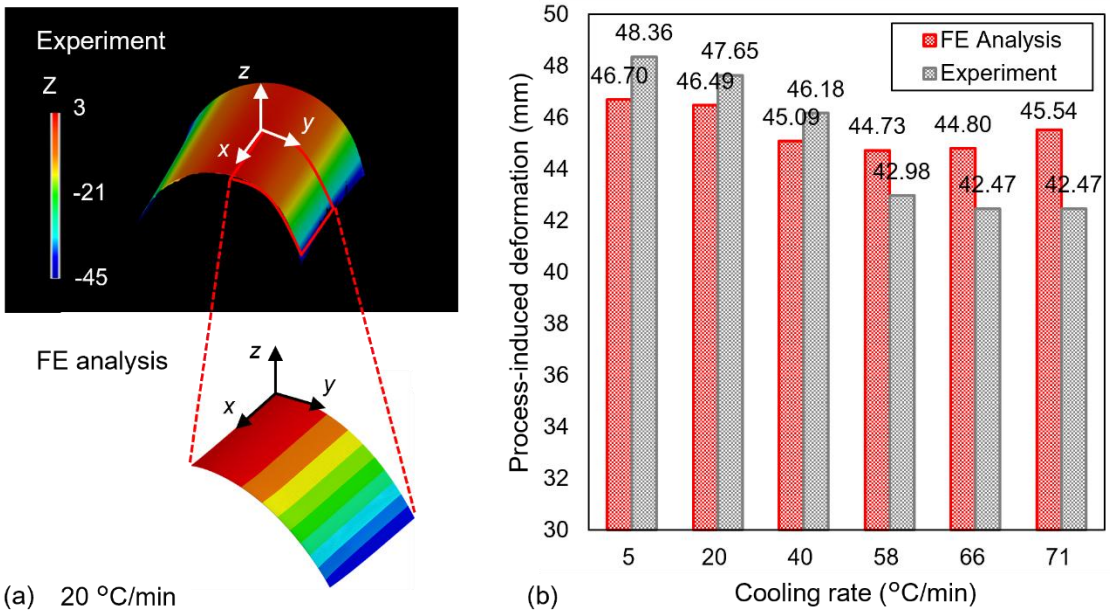

Figure 5. Comparison between experimental and numerical PID results in T700G/LM-PAEK cross-ply laminates: (a) out-of-plane deformation distribution; (b) PID values at different cooling rates.

Although the experimentally observed trend was captured, more accurate prediction requires further consideration of the temperature at which the CFRTP laminate begins to develop stiffness during cooling. To examine this point, additional DSC measurements were conducted on T700G/LM-PAEK prepregs over a temperature range of 20–365 °C at a heating rate of 80 °C/min, followed by cooling at rates of 1, 5, 8, 20, and 70 °C/min. Figure 6 shows the resulting DSC cooling

curves, each of which exhibited an exothermic peak associated with crystallization. When the crystallization onset temperature was defined as the temperature at which the exothermic peak began to deviate from the baseline, the onset temperature decreased with increasing cooling rate. This decrease can be attributed to the temperature drop at higher cooling rates before sufficient nucleation and crystal growth can occur. Therefore, the stiffness-development temperature is expected to decrease at higher cooling rates, further reducing residual stress. In the present analysis, this temperature was assumed to be constant; incorporating its cooling-rate dependence is expected to further improve the accuracy of PID prediction.

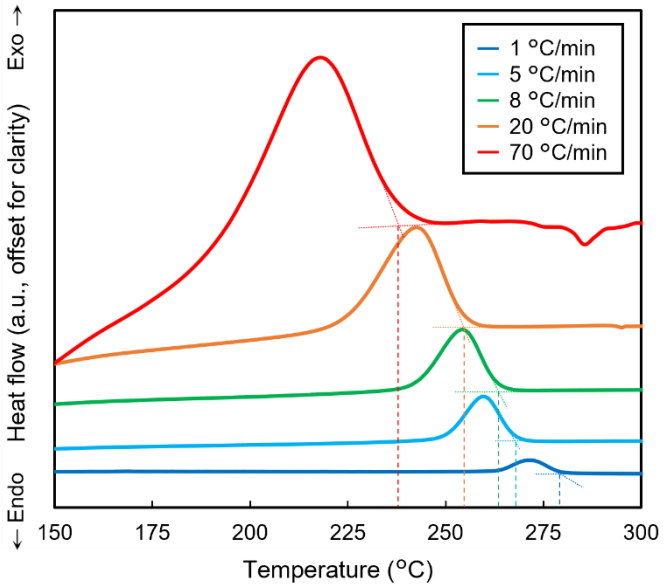

Figure 6. DSC cooling curves of T700G/LM-PAEK prepregs measured at different cooling rates. The curves are vertically shifted for clarity, and only the crystallization onset temperature is compared.

5. Conclusions

This study investigated the cooling-rate-dependent PID of T700G/LM-PAEK thermoplastic composite laminates through experiments and FE analysis. Laminates were fabricated under six cooling-rate conditions, and their PID, crystallinity, and viscoelastic properties were evaluated using three-dimensional scanning, DSC, and DMA. The degree of crystallinity and initial stiffness decreased with increasing cooling rate, leading to a reduction in PID. An anisotropic viscoelastic FE analysis incorporating cooling-rate-dependent stiffness and crystallization-induced shrinkage reproduced the experimentally observed decrease in PID with increasing cooling rate. The results indicate that the reduction in crystallinity at higher cooling rates lowers both the laminate stiffness and crystallization-induced shrinkage strain, thereby reducing residual stress. Additional DSC measurements showed that the crystallization onset temperature also decreases with increasing cooling rate, suggesting that the temperature at which the laminate begins to develop stiffness should be considered for more accurate PID prediction.

Acknowledgments

This study was supported by JSPS KAKENHI Grant Numbers JP23K19085 and JP24K17167. This study was also based on results obtained from a project, JPNP25004, commissioned by the New Energy and Industrial Technology Development Organization (NEDO). The authors gratefully acknowledge Mr. Junichi Go and Mr. Umito Yoshioka (Go Factory Co., Ltd.) for their technical assistance during the fabrication of the thermoplastic composite laminates.

References

[1] P.P. Parlevliet, H.E.N. Bersee and A. Beukers. "Residual stresses in thermoplastic composites—A study of the literature—Part I: Formation of residual stresses". *Composites Part A: Applied Science and Manufacturing*, Vol.37, No.11, pp.1847–1857, 2006.

[2] E. Barocio, J. Hicks, G. Kim, A. Favaloro, G. Ghosh, J. Goodsell and R. B. Pipes, "Validation of shape change predictions for stamp forming of carbon fiber thermoplastic composite laminates". *Composites Part B: Engineering*, Vol.275, Paper No.111325, 2024.

[3] K. Ryuzono, S. Koo, Y. Hoshikawa, Y. Kawagoe and T. Okabe. "Mechanism investigation and comparison of long-term deformations caused by process-induced residual stresses in thermosetting CF/epoxy and thermoplastic CF/PAEK composite laminates". *Composites Part A: Applied Science and Manufacturing*, Vol.196, Paper No.108963, 2025.

[4] S. Koo, Y. Hoshikawa, Y. Kawagoe, K. Ryuzono and T. Okabe. "Process-induced residual stress in non-crimp fabric composites: Experimental and numerical evaluation considering viscoelasticity". *Mechanics of Materials*, Vol. 209, Paper No.105423, 2025,

[5] M. Golzar, J. Sinke and M. Abouhamzeh. "Novel thermomechanical characterization for shrinkage evolution of unidirectional semi-crystalline thermoplastic prepregs (PPS/CF) in melt, rubbery and glassy states". *Composites Part A: Applied Science and Manufacturing*, Vol.156, Paper No.106879, 2022.

[6] J. Zhang, G. Liu, P. An, K. Yu, J. Huang, Y. Gu, J. Yao, R. Cao, H. Liu, C. Chen, C. Zhang and M. Wang. "The effect of cooling rates on crystallization and low-velocity impact behaviour of carbon fibre reinforced poly(aryl ether ketone) composites". *Composites Part B: Engineering*, Vol.254, Paper No.110569, 2023.

[7] S. Oshima, R. Higuchi, M. Kato, S. Minakuchi, T. Yokozeki and T. Aoki. "Cooling rate-dependent mechanical properties of polyphenylene sulfide (PPS) and carbon fiber reinforced PPS (CF/PPS)". *Composites Part A: Applied Science and Manufacturing*, Vol.164, Paper No.107250, 2023.

[8] D.J. Blundell and B.N. Osborn. "The morphology of poly(aryl-ether-ether-ketone)". *Polymer*, Vol.24, No.8, pp.953–958, 1983.

[9] Toray Advanced Composites. Toray Cetex TC1225 Data Sheet. 2026. (Accessed June 1 2026).

[10] W. Chen and D. Zhang. "Improved prediction of residual stress induced warpage in thermoset composites using a multiscale thermo-viscoelastic processing model". *Composites Part A: Applied Science and Manufacturing*, Vol.126, Paper No.105575, 2019.

[11] K. Kashmari, H.A. Mahmud, S.U. Patil, W.A. Pisani, P. Deshpande, M. Maiaru and G. M. Odegard, "Multiscale process modeling of semicrystalline PEEK for tailored thermomechanical properties". *ACS Applied Engineering Materials*, Vol.1(11), pp.3167–3177, 2023.